Chaos, Solitons and Fractals 183 (2024) 114915

Contents lists available at ScienceDirect

Chaos, Solitons and Fractals

journal homepage: www.elsevier.com/locate/chaos

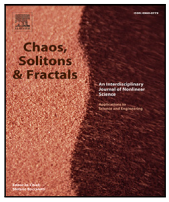

Electronic implementation of simplicial complexes

V.P. Vera-Ávila [a], R.R. Rivera-Durón [b], Miguel S. Soriano-Garcia [b], R. Sevilla-Escoboza [b,*], Javier M. Buldú [c]

[a] Instituto Politécnico Nacional, Unidad Profesional Interdisciplinaria de Ingeniería Campus Guanajuato, Av. Mineral de Valenciana 200, C. Industrial Puerto Interior, Silao, 36275, Guanajuato, Mexico
[b] Centro Universitario de los Lagos, Universidad de Guadalajara, Enrique Díaz de León, Paseos de la Montaña, Lagos de Moreno, 47460, Jalisco, Mexico
[c] Complex Systems Group and G.I.S.C., King Juan Carlos University, Calle Tulipán s/n, Móstoles, 28933, Madrid, Spain

ARTICLE INFO

Keywords:
Synchronization
Complex networks
Simplicial complexes
Electronic circuits

ABSTRACT

We design an experimental implementation of a simplicial complex, a complex network structure with higher-order interactions between nodes. Using a set of three Rössler-like (analog) electronic circuits under a chaotic dynamical regime, we demonstrate how the synchronization basin is enhanced by introducing higher-order interactions between the triplet of nodes, as suggested in recent theoretical works. The experiments prove that, when the coupling is introduced through the adequate variable, the synchronization area is increased. The combination of pairwise (i.e., node-to-node) with high-order (i.e., triplet) coupling is analyzed by modifying the corresponding coupling strengths, σ_1 and σ_2. Importantly, we detail the procedure for reproducing the experimental setup and provide all datasets generated in the laboratory, in order to allow other researchers to further investigate the properties of complex networks with higher-order interactions.

1. Introduction

A large number of physical, chemical, biological systems can be modeled using networks of units that interact with each other. These units can be described as dynamical systems, where their evolution over time is influenced by the states of other units that are connected through the links of the network. Understanding how this interaction constrains the dynamics of the individual systems and, at the same time, the collective behavior of the network is a problem of great interest between different disciplines [1,2].

To understand these phenomena, network science is used, where the study focuses not on the element in a particular way but to the response in conjunction of all those elements that make up the network [2]. Brain networks [3,4], the interaction between proteins [5], semantic networks [6] or academic collaborations [7] are some practical situations where the analysis of the interactions is crucial to understand the functioning of the whole system.

In the realm of network science, the exploration of simplicial complexes has marked a significant departure from traditional network analysis, offering a richer and more comprehensive view of complex systems [8,9]. Simplicial complexes are mathematical structures that capture higher-order relationships among nodes, edges, triangles, and beyond that, they have opened new frontiers for understanding the intricate web of connections within a wide range of systems [10]. Traditional network models, such as graphs, focus on pairwise interactions between nodes. However, simplicial complexes go beyond this by considering higher-order interactions involving more than two nodes [11]. This higher-order perspective is crucial for capturing the complexity and richness of real-world networks [12–14]. One application of simplicial complexes is in modeling of social contagion. In this way, Iacopini et al. (2019) introduced a higher-order model of social contagion using simplicial complexes, where interactions can occur within groups of different sizes [15]. This approach provided a more realistic representation of how contagion spreads in social systems. Furthermore, simplicial complexes have been used to study the spectrum of complex networks. Reitz & Bianconi (2020) presented a renormalization group approach to analyze the higher-order spectrum of simplicial complexes [16], allowing for a deeper understanding of the collective behavior and dynamics of complex systems. The configuration model and the canonical ensemble of simplicial complexes have also been proposed in [17]. These generalized network structures provide a framework for studying a wide range of complex interacting systems, including brain networks and collaboration networks. Weighted growing simplicial complexes have also been investigated by Courtney & Bianconi [18]. This research explored network structures where interactions can involve more than two nodes. Such weighted simplicial complexes have been found to accurately describe collaboration networks, protein interaction networks, and brain networks.

* Corresponding author.
E-mail address: jesus.escoboza@academicos.udg.mx (R. Sevilla-Escoboza).

https://doi.org/10.1016/j.chaos.2024.114915
Received 25 January 2024; Received in revised form 18 April 2024; Accepted 19 April 2024
Available online 8 May 2024

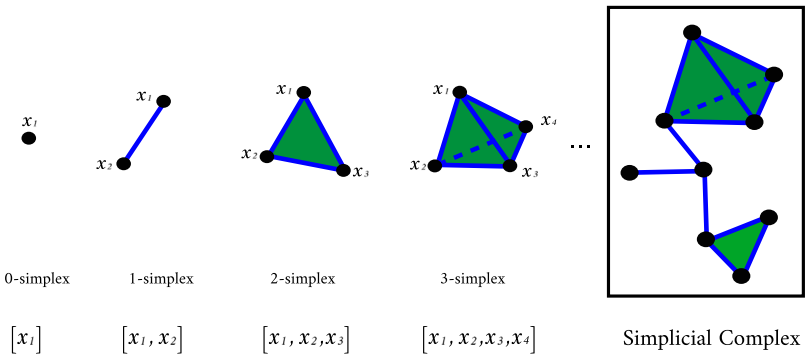

Fig. 1. Different type of simplex structures according to the dimension D, to the generation of simplicial complex: 0-simplex (point or node), 1-simplex (line or link), 2-simplex (triangle or triplet), 3-simplex (tetrahedra).

In addition to their structural properties, simplicial complexes have also been studied in the context of network geometry. Bianconi & Rahmede (2017) investigated the emergent hyperbolic network geometry of simplicial complexes [11]. This research revealed the underlying geometric properties of complex networks and their relationship to simplicial complexes. Finally, the higher-order spectral dimension and dynamics of simplicial complexes have been explored by (Torres & Bianconi, 2020) [19], highlighting the importance of considering the dimensionality of simplicial complexes in understanding the behavior and evolution of complex systems.

More recently, Gambuzza et al. presented a general framework for analyzing the stability of the complete synchronization state in simplicial complexes with multiple interaction layers [20]. They highlighted the importance of topology and geometry in determining the dynamical properties of simplicial complexes [21]. The paper contributed to the understanding of synchronization in complex networks and provided insights into the stability of synchronization in simplicial complexes by extending the formulation of a Master Stability Function (MSF) to networks with higher-order interactions. The MSF formulation allows to assess the linear stability of the (complete) synchronization manifold of a set of coupled identical dynamical systems, just by taking into account the equations of the dynamical system and the kind of coupling [22].

Departing from the theoretical results of Gambuzza et al. [20], in this paper we provide the first experimental implementation of a network of dynamical simplicial complexes. This endeavor brings together theoretical insights, computational techniques, and practical experimentation to bridge the gap between mathematical constructs and tangible, real-world networks. Specifically, we depart from 3 electronic Rössler systems evolving with a chaotic dynamics. Next, we couple them through (i) pairwise and (ii) high-order (2-simplex) coupling and investigate how the coupling strength constrains the synchronization manifold of the three dynamical systems. Our analysis include coupling through different variables of the Rössler systems and show how the combination of the two kind of couplings allows different ways of achieving the synchronization manifold. Importantly, together with the results we provide the detailed schematic designs of the electronic circuits and a database containing the dynamics of the oscillators under all possible coupling scenarios.

2. Theoretical framework

A simplicial complex is formed by a collection of simplices, which are geometric objects of different dimensions. In the context of network science, these simplices represent interactions or connections between nodes. Under this framework, a node of the network is a 0-dimensional simplex and a link is a 1-dimensional simplex connecting two nodes and representing a pairwise interaction or relationship. We can go to higher order interactions and define a triangle as a 2-dimensional simplex formed by connecting three nodes and a tetrahedron as a 3-dimensional simplex formed by connecting four nodes. Applying the same reasoning, higher-dimensional simplices represent interactions involving more nodes (see Fig. 1 for details). The collection of all these simplices, along with their shared faces, forms the simplicial complex. Importantly, if k at $\mathbb{R}^n$ is a collection of *simplices* at $\mathbb{R}^n$, then the intersection of every two *simplices* of k is one face of each of them. Note that, in the case of dimension $D \leq 1$, the simplicial complex coincides with the standard case of a complex network of N units coupled through pairwise interactions (i.e., links connect two, and only two, nodes).

In the same spirit as [20], let us consider a dynamical system to be placed at each of the N nodes of a simplicial complex of dimension D, the equations that describe its evolution are:

$$\begin{aligned}\dot{\mathbf{x}}_i &= \mathbf{f}(\mathbf{x}_i) + \sigma_1 \sum_{j_1=1}^{N} a^{(1)}_{i,j_1} \mathbf{g}^{(1)}(\mathbf{x}_i, \mathbf{x}_{j_1}) \\ &+ \sigma_2 \sum_{j_1=1}^{N}\sum_{j_2=1}^{N} a^{(2)}_{i,j_1,j_2} \mathbf{g}^{(2)}(\mathbf{x}_i, \mathbf{x}_{j_1}, \mathbf{x}_{j_2}) + \cdots \\ &+ \sigma_D \sum_{j_1=1}^{N} \cdots \sum_{j_D=1}^{N} a^{(D)}_{i,j_1,\ldots,j_D} \mathbf{g}^{(D)}(\mathbf{x}_i, \mathbf{x}_{j_1}, \ldots, \mathbf{x}_{j_D}),\end{aligned} \tag{1}$$

where $\mathbf{x}_i(t)$ is a m-dimensional vector describing the dynamics of node i and $\sigma_1, \ldots, \sigma_D$ are the coupling strengths of each D-dimensional simplex. The function $\mathbf{f} : \mathbb{R}^m \to \mathbb{R}^m$ describes the local dynamics, which is assumed identical to all units, while $\mathbf{g}^d : \mathbb{R}^{(d+1)\times m} \to \mathbb{R}^m$ ($d = 1, \ldots, D$) (i.e. $g^d(\mathbf{x}, \mathbf{x}, \ldots, \mathbf{x}) \equiv 0 \ \forall d$) are synchronization functions describing the kind of interaction at different orders. In addition $a^{(d)}_{i,j_1,\ldots,j_d}$ are the entries of adjacency tensors A^d, using $d = 1, \ldots, D$. These tensors, which generalize the notion of adjacency matrix of a graph, describe the architecture of the interactions of any order that can take place in the simplicial complexes. Note the generality of the equation, since there are no additional specific restrictions both in the adjacency tensors of the simplicial complex and the functions $\mathbf{f}$ and $\mathbf{g}^{(D)}$.

3. Constructing electronic simplicial complexes

The main objective of this paper is to construct a simplicial complex composed of nonlinear electronic circuits, with the aim of exploring its synchronization abilities. The construction of the experimental setup consists of two stages: (i) the implementation of a set of nonlinear electronic oscillators and (ii) the construction of the simplicial complex. Regarding the first stage, each node consisted of an electronic Rössler oscillator [23–25], which was constructed using analog devices (operational amplifiers), passive elements (resistors, variable resistors, capacitors), and some specific purpose integrated circuits (multipliers). We used the operational amplifier LM324N to construct the equations and the integrators, which is a low-power integrated circuit. This integrated circuit includes four amplifiers to implement all the conventional operational amplifiers configurations and gain blocks. Fig. 2 shows the schematics of the electronic Rössler.

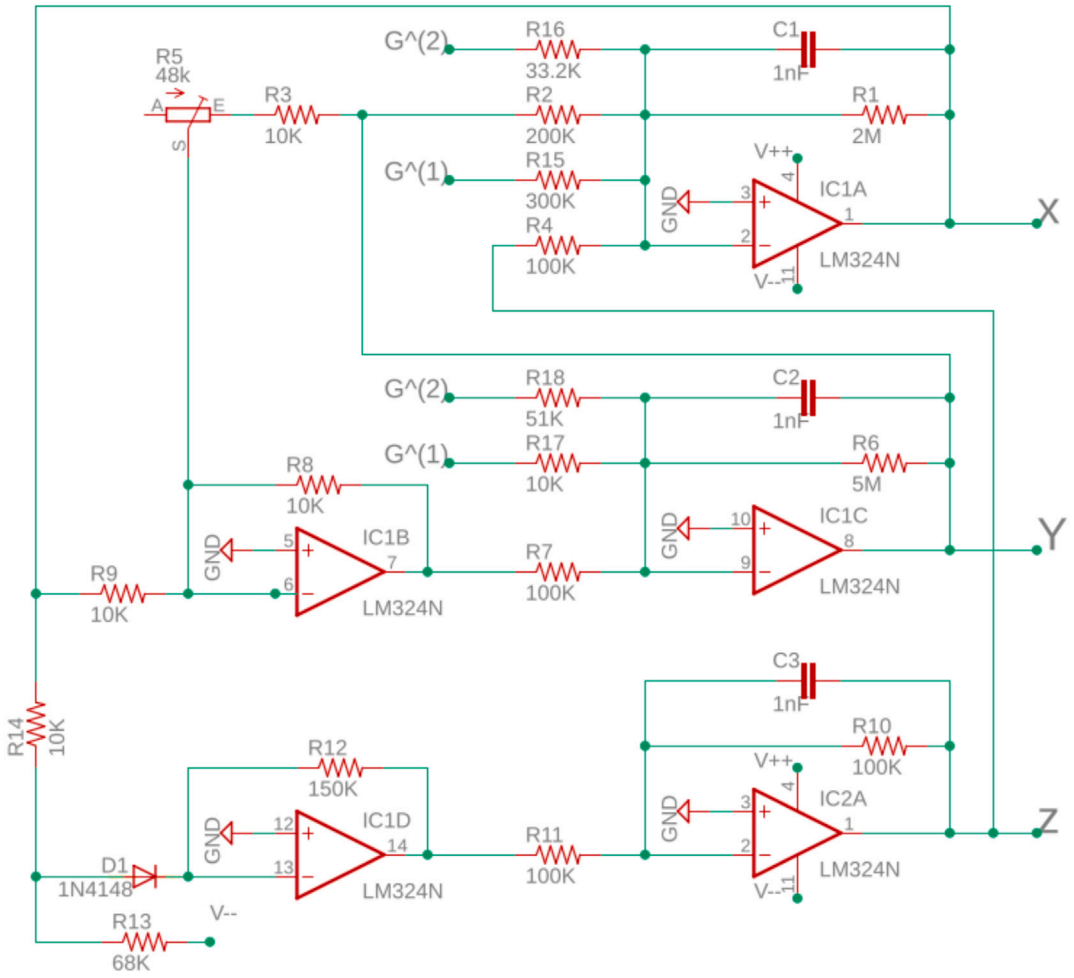

Fig. 2. Experimental design of an electronic Rössler oscillator. The oscillator is constructed using operational amplifiers (LM324N), passive elements (R: resistors, C: capacitors), and diodes (D).

The equations describing the dynamics of the electronic Rössler oscillator depicted in Fig. 2 are:

$$\dot{x} = -\frac{1}{R_1 C_1}\left(x + \frac{R_1}{R_2}y + \frac{R_1}{R_4}z\right) \tag{2}$$

$$\dot{y} = -\frac{1}{R_6 C_2}\left(-\frac{R_6 R_8}{R_9 R_7}x + \left[1 - \frac{R_6 R_8}{R_C R_7}\right]y\right) \tag{3}$$

$$\dot{z} = -\frac{1}{R_{10} C_3}\left(-\frac{R_{10}}{R_{11}}G_x + z\right), \tag{4}$$

where x, y and z are the voltages at the output of the three operational amplifiers IC1 A, IC1C and IC2 A (see Fig. 2 for details) and G_x is a nonlinear gain function given by:

$$G_x = \begin{cases} 0 & x \le V_d + V_d\frac{R_{14}}{R_{13}} + V_{ee}\frac{R_{14}}{R_{13}} \\ \frac{R_{12}}{R_{14}}x - V_{ee}\frac{R_{12}}{R_{13}} - V_d\left(\frac{R_{12}}{R_{14}} + \frac{R_{12}}{R_{13}}\right) & x > V_d + V_d\frac{R_{14}}{R_{13}} + V_{ee}\frac{R_{14}}{R_{13}}. \end{cases} \tag{5}$$

To ensure that the oscillators are as identical as possible, we used 1% precision resistors and adjusted the variable resistors to guarantee the oscillators display the same dynamics, which was verified by means of the frequency spectrum. We set all oscillators to have chaotic dynamics by adjusting the electronic components to the values shown in Table 1.

Next, we constructed a simplicial complex with dimension $D = 2$ using $N = 3$ electronic Rösslers, which corresponds to the smallest simplicial complex of this dimension. Taking the equations of Rössler oscillator, we considered two different coupling scenarios, the first one using x_i as the coupling variable of an oscillator i (with $i = 1, 2, 3$)

Table 1
Values of the electronic components of Fig. 2. Under these conditions, the electronic Rössler oscillators have chaotic dynamics.

$C_{1-3} = 1$ nF	$V_d = 0.7$	$V_{ee} = 9$	$R_C = R_3 + R_5$
$R_1 = 2$ MΩ	$R_2 = 200$ kΩ	$R_3 = 10$ kΩ	$R_4 = 100$ kΩ
$R_5 = 48$ kΩ	$R_6 = 5$ MΩ	$R_7 = 100$ kΩ	$R_8 = 10$ kΩ
$R_9 = 10$ kΩ	$R_{10} = 100$ kΩ	$R_{11} = 100$ kΩ	$R_{12} = 150$ kΩ
$R_{13} = 68$ kΩ	$R_{14} = 10$ kΩ	$R_{15} = 300$ kΩ	$R_{16} = 33.2$ kΩ
$R_{17} = 10$ kΩ	$R_{18} = 51$ kΩ	$\sigma_1 = [0-2]Vcc$	$\sigma_2 = [0-0.02]Vcc$

and the second one, using the y_i variable. Specifically, the coupling functions for the x_i variable were $g^{(1)}(\mathbf{x}_i, \mathbf{x}_j) = [x_j - x_i, 0, 0]^T$ and $g^{(2)}(\mathbf{x}_i, \mathbf{x}_j, \mathbf{x}_k) = [x_j^2 x_k - x_i^3, 0, 0]^T$. Similarly, for the y_i variable, the coupling functions were $g^{(1)}(\mathbf{y}_i, \mathbf{y}_j) = [y_j - y_i, 0, 0]^T$ and $g^{(2)}(\mathbf{y}_i, \mathbf{y}_j, \mathbf{y}_k) = [y_j^2 y_k - y_i^3, 0, 0]^T$. Both $g^{(1)}$ and $g^{(2)}$ represent generalized diffusion functions. In the case of $g^{(1)}$, it is the simplest diffusive function which relates the state of node i with the node j. For the case of $g^{(2)}$, it was built considering the smallest power function that involves the three nodes without redundancies. In other words, $g^{(2)}$ is the difference between two monomials with the same degree, in this case, third degree. Note that, to achieve identical synchronization, the two coupling functions $g^{(1)}$ and $g^{(2)}$ must be constructed in a way that when $\mathbf{x}_i = \mathbf{x}_j = \mathbf{x}_k$, the coupling terms go to zero. It is important to mention two fundamental aspects, the first one is the fact that we are using the same coupling functions proposed by Gambuzza et al. in [20]; and the second one is that we are not using the z_i variable for coupling, this obeys

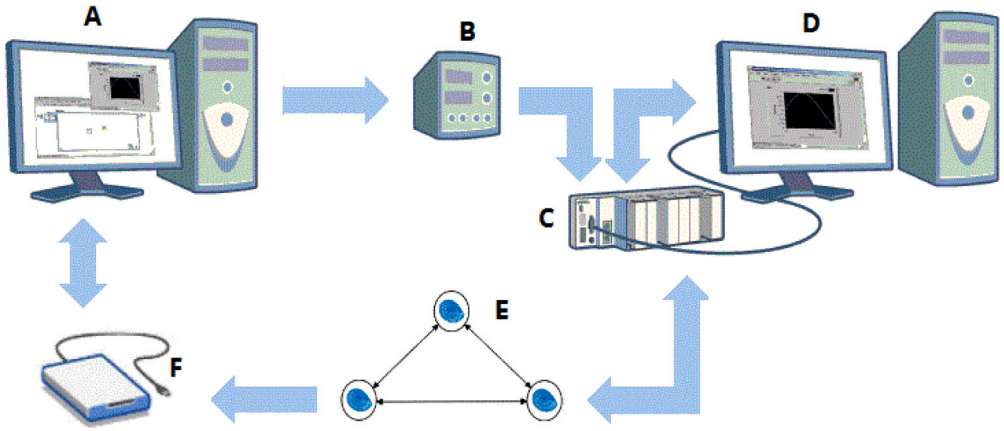

Fig. 3. Schematic representation of the experimental setup. (A) Labview code controlling the coupling strengths σ_1 and σ_2 and storing the outputs of the simplicial complex. (B) Two-channel programmable power supply. (C) Analog module CompaqRIO reading the state variables and introducing the coupling functions. (D) Labview code calculating the coupling functions. (E) Analog simplicial complex composed of 3 Rössler oscillators. (F) Data acquisition card capturing the outputs of the simplicial complex.

to the knowledge that Rössler system does not synchronize when it is coupled through the z variable because the Master Stability Function corresponds to the Class I according with the classification presented in [26]. Introducing the aforementioned coupling terms in Eqs. (2)–(4), we obtain the equations of the simplicial complex:

$$\dot{x}_i = -\frac{1}{R_1 C_1}\left(x_i + \frac{R_1}{R_2}y_i + \frac{R_1}{R_4}z_i - \sigma_1\frac{R_1}{R_{15}}\sum_{j=1}^{N} g_{ij}^{(1)}(x_j - x_i)\right) - \frac{1}{R_1 C_1}\left(-\sigma_2\frac{R_1}{R_{16}}\sum_{j=1}^{N}\sum_{k=1}^{N} g_{ijk}^{(2)}(x_j^2 x_k - x_i^3)\right) \tag{6}$$

$$\dot{y}_i = -\frac{1}{R_6 C_2}\left(-\frac{R_6 R_8}{R_9 R_7}x_i + \left[1 - \frac{R_6 R_8}{R_C R_7}\right]y_i - \sigma_1\frac{R_6 R_8}{R_{17} R_7}\sum_{j=1}^{N} g_{ij}^{(1)}(y_j - y_i)\right) - \frac{1}{R_6 C_2}\left(-\sigma_2\frac{R_6 R_8}{R_{18} R_7}\sum_{j=1}^{N}\sum_{k=1}^{N} g_{ijk}^{(2)}(y_j^2 y_k - y_i^3)\right) \tag{7}$$

$$\dot{z}_i = -\frac{1}{R_{10} C_3}\left(-\frac{R_{10}}{R_{11}}G_{x_i} + z_i\right). \tag{8}$$

4. Coupling control and recording

Fig. 3 shows a qualitative representation of the complete experimental setup. The fact that we wanted to combine and control, at the same time, the coupling of dimensions 1 and 2, required to consider two varying coupling strengths σ_1 and σ_2, the former for the 1-simplex (i.e., single links) and the latter for the 2-simplex (i.e., triplets). With this aim, we used a two-channel programmable power supply model GW Instek GPD 2003S (B), whose two output voltages directly controlled the values of σ_1 and σ_2. Next, with the aim of plotting the synchronization error map, each coupling strength was modified 100 times through a Labview code (A) that controls a programmable power supply (B), in such a way that when the complete experiment was finished, we obtained 100 × 100 time series for each of the three nodes of the simplicial complex. The values of σ_1, σ_2, and two state variables of the three nodes (x_i and y_i) were recorded simultaneously by an analog inputs module NI 9201 of CompaqRIO embedded system (C). In real-time, these input signals are processed by another Labview program (D) that calculates the coupling functions $g^{(1)}$ and $g^{(2)}$. After the terms of the linear diffusive coupling function $g^{(1)}$ and the high-order coupling function $g^{(2)}$ have been calculated, they were fed back to the electronic oscillators (E) through the analog outputs module NI 9264 of the CompaqRIO (C). Finally, a data acquisition card (F) captured the temporal series of the Rösslers and sends them to a Labview program (A) that stores them in the hard disk to be processed later using Matlab.

The data acquisition card we used is the USB-6363 of National Instruments, whose Analog-to-Digital Converter and Digital-to-Analog converter works at 16-bit. This implies that if we are using analog signals from the range of −9 V to 9 V, the voltage for each possible code of 16-bit is around 274.6 μV. On the other hand, this device collects data on all channel in sequential order using a multiplexer. The settling time to achieve this task is 1 to 2 μs. This delay time is much less than the oscillation frequency of Rössler system, which is around 1.5 kHz. The sequential order to collect data from the analog inputs in our setup is 3-4-2-5-1-0, remembering that analog inputs are labeled from 0 to 7 in the data acquisition card. The delay to acquire these six signals is around 10 μs. The model of CompaqRIO embedded system we used is 9074, which has a sample rate of 10 kS/s when is working in FPGA mode. The existing delay between the measurement and the application of a perturbation is approximately 5 μs.

An important point to note is the hybrid character of our experimental platform, since we used analog and digital devices jointly. Analog devices were present in the Rössler oscillators, whereas the digital devices carried out the calculation of the coupling functions $g^{(1)}$ and $g^{(2)}$ using the real-time processor and the FPGA modules of the CompaqRIO. If the complete experiment had been implemented using only analog devices, the cost and complexity of the circuit had increased. Just to cite an example, if the full experiment were implemented using only analog electronic devices, for each high-order coupling function $g^{(2)}$, a total of 18 multipliers would be necessary. Note that these devices are the most expensive components for constructing the experiment, in such a way that we estimate the cost would increase 15 times with respect to our hybrid experimental platform.

5. Results

We carried out four experiments to consider all the possible combinations of the coupling functions $g^{(1)}$ and $g^{(2)}$ through the state variables x_i and y_i: (i) $g^{(1)} \to x_i$ and $g^{(2)} \to x_i$, (ii) $g^{(1)} \to x_i$ and $g^{(2)} \to y_i$, (iii) $g^{(1)} \to y_i$ and $g^{(2)} \to x_i$ and (iv) $g^{(1)} \to y_i$ and $g^{(2)} \to y_i$. Variable z_i is not included here since we observed that the synchronization manifold is never reached when oscillators are coupled through this variable. For each experiment, we calculate the synchronization error of the recorded variables as:

$$E = \left\langle \left(\frac{1}{N(N-1)} \sum_{i,j=1}^{N} \|\mathbf{x}_j - \mathbf{x}_i\|^2 \right)^{\frac{1}{2}} \right\rangle \tag{9}$$

where $\|\cdot\|$ is the absolute value and $\langle\cdot\rangle$ is the average over time. Figs. 4–7 contain maps of the synchronization error for each experiment. In these maps, the color bar indicates how synchronized the

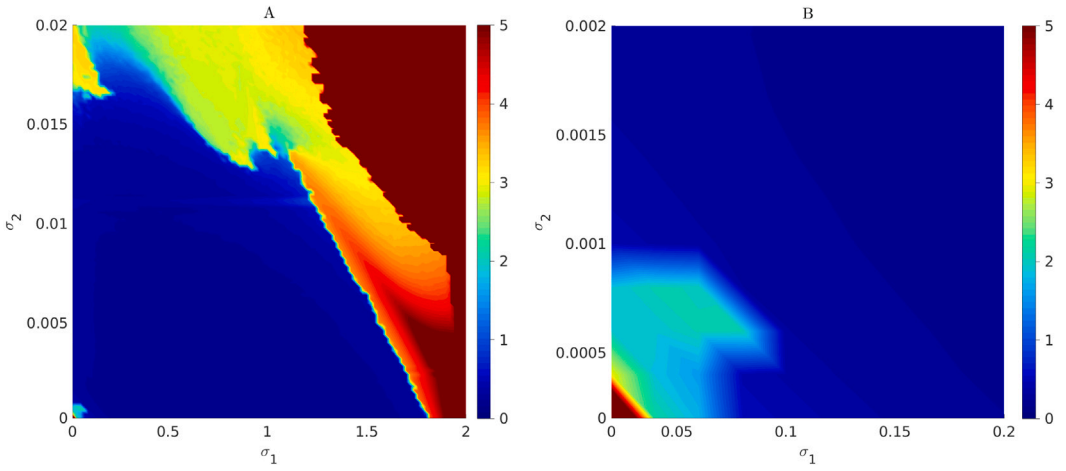

Fig. 4. Synchronization error map for $g^{(1)}(\mathbf{x}_i, \mathbf{x}_j) = [x_j - x_i, 0, 0]^T$ and $g^{(2)}(\mathbf{x}_i, \mathbf{x}_j, \mathbf{x}_k) = [x_j^2 x_k - x_i^3, 0, 0]^T$ as a function of the coupling strengths σ_1 and σ_2. (A) Full range experiment. (B) Zoom of plot A for low coupling strengths. This plot corresponds to the experiment (i) referred in the main text. (For interpretation of the references to color in this figure legend, the reader is referred to the web version of this article.)

network is. The scale goes from the blue tones to the red tones, which correspond to the synchronized state and non-synchronized state, respectively. With the aim of better elucidating each of the aforementioned scenarios, we also have included maps of the synchronization error calculated by numerical simulations (Supplementary Material Section). Fig. 4 shows the synchronization error maps of experiment (i), where we introduced the couplings through the x_i variable as $g^{(1)}(\mathbf{x}_i, \mathbf{x}_j) = [x_j - x_i, 0, 0]^T$ and $g^{(2)}(\mathbf{x}_i, \mathbf{x}_j, \mathbf{x}_k) = [x_j^2 x_k - x_i^3, 0, 0]^T$. Panel B shows a zoom of panel A for low values of coupling. We can observe how, for values of σ_1 close to zero, there is no synchronized state (see panel B), but when σ_1 is slightly increased, the system reaches the synchronization manifold. However, the network loses again the synchronized state as σ_1 is increased beyond $\sigma_1 = 1.80$. The same qualitative behavior can be seen for σ_2 when σ_1 is set to zero. It is worth noting how the combination of both coupling strengths leads to a region where the synchronization manifold is lost before the case of coupling the oscillators with only a coupling of a given order (either $g^{(1)}$ or $g^{(2)}$). In other words, coupling through the two variables at the same times does not promote synchronization, on the contrary, makes the system to leave the synchronization region more easily. This is the classical behavior of the class III systems defined by the Master Stability Function (MSF) in the context of complex networks with (only) pairwise interactions [26].

The second experiment corresponds to $g^{(1)} = (\mathbf{x}_i, \mathbf{x}_j) = [x_j - x_i, 0, 0]^T$ and $g^{(2)} = (\mathbf{x}_i, \mathbf{x}_j, \mathbf{x}_k) = [0, y_j^2 y_k - y_i^3, 0]^T$, whose synchronization error map is sketched in Fig. 5. In this case, introduced the high-order interaction through the y_i variable, combining the use of two variables at the same time. We can observe how, when both σ_1 and $\sigma_2 = 0$, the simplicial complex displays asynchronous dynamics. This is an expected behavior because there is not coupling between them. However, as soon as σ_1 starts to increase, the ensemble fully synchronizes. The asynchronous behavior appears again in the network when σ_1 is, again, higher than 1.80 when σ_2 is set to zero. If we keep $\sigma_1 = 0$ and analyze the effects of increasing σ_2, we can see that the behavior is qualitatively similar. However, σ_2 requires to reach a higher value to enter the synchronization region than in the case of experiment (i), where the coupling $g^{(2)}$ was introduced through the x_i variable. Also note that, now synchronization is maintained even for high values of both σ_1 and σ_2. This is a behavior that is similar to class II systems, as defined by the Master Stability Function [26].

In experiment (iii) coupling functions are $g^{(1)} = (\mathbf{x}_i, \mathbf{x}_j) = [0, y_j - y_i, 0]^T$ and $g^{(2)} = (\mathbf{x}_i, \mathbf{x}_j, \mathbf{x}_k) = [x_j^2 x_k - x_i^3, 0, 0]^T$. Here, we have exchanged the coupling variables as compared to experiment (ii), maintaining a multivariable coupling. We can observe in Fig. 6 how the asynchronous behavior appears when both σ_1 and σ_2 are small, but as we increment

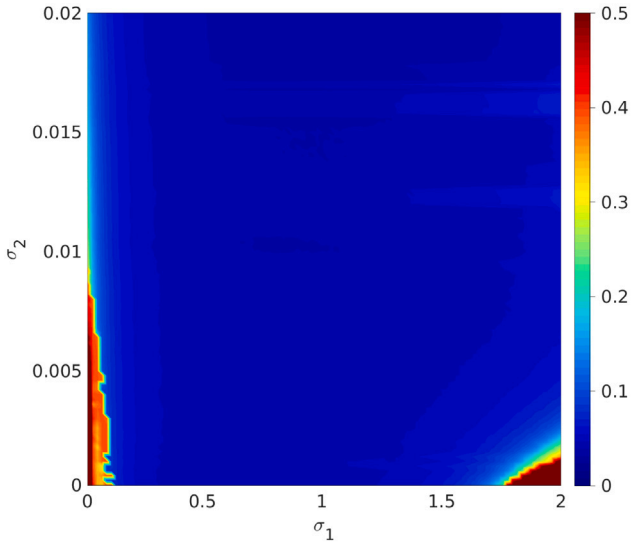

Fig. 5. Synchronization error map for $g^{(1)} = (\mathbf{x}_i, \mathbf{x}_j) = [x_j - x_i, 0, 0]^T$ and $g^{(2)} = (\mathbf{x}_i, \mathbf{x}_j, \mathbf{x}_k) = [0, y_j^2 y_k - y_i^3, 0]^T$ as a function of the coupling strengths σ_1 and σ_2. This plot corresponds to the experiment (ii) referred in the main text. (For interpretation of the references to color in this figure legend, the reader is referred to the web version of this article.)

σ_2, the network reaches the synchronization manifold. Nevertheless, if we continue increasing σ_2 and we let σ_1 small, then the network loses again the synchronized behavior.

Finally, in experiment (iv), the coupling is fully introduced through the y_i variable in such a way that *i.e.*, $g^{(1)} = (\mathbf{x}_i, \mathbf{x}_j) = [0, y_j - y_i, 0]^T$ and $g^{(2)} = (\mathbf{x}_i, \mathbf{x}_j, \mathbf{x}_k) = [0, y_j^2 y_k - y_i^3, 0]^T$. Fig. 7 shows how, in this configuration, the asynchronous behavior of the simplicial complex only exists for small values of σ_1 and σ_2. When a certain threshold value is crossed for σ_1 and σ_2, the synchronization region is always reached even for high values of both couplings.

6. Conclusions

In this paper we presented the first experimental results of a simplicial complex composed of nonlinear electronic oscillators. Our main aim was to design an experimental setup able to analyze all possible scenarios to reach the synchronized state of a simplicial complex by modifying its coupling strengths. Our setup consisted on a hybrid

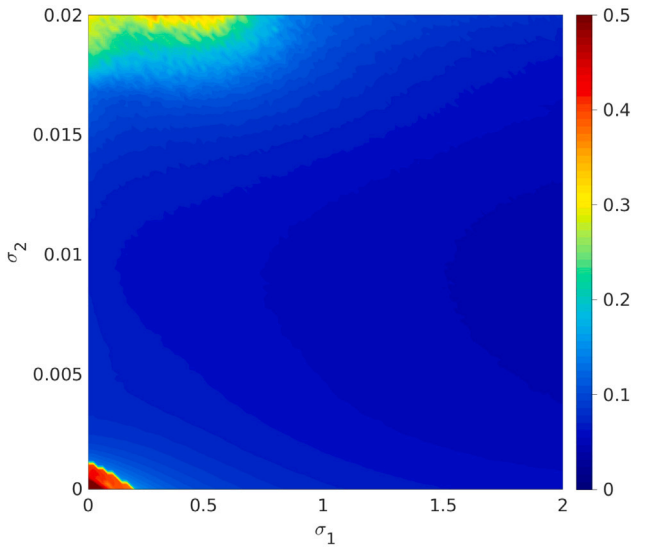

Fig. 6. Synchronization error map for $g^{(1)} = (\mathbf{x}_i, \mathbf{x}_j) = [0, y_j - y_i, 0]^T$ and $g^{(2)} = (\mathbf{x}_i, \mathbf{x}_j, \mathbf{x}_k) = [x_j^2 x_k - x_i^3, 0, 0]^T$ as a function of the coupling strengths σ_1 and σ_2. This plot corresponds to the experiment (iii) referred in the main text. (For interpretation of the references to color in this figure legend, the reader is referred to the web version of this article.)

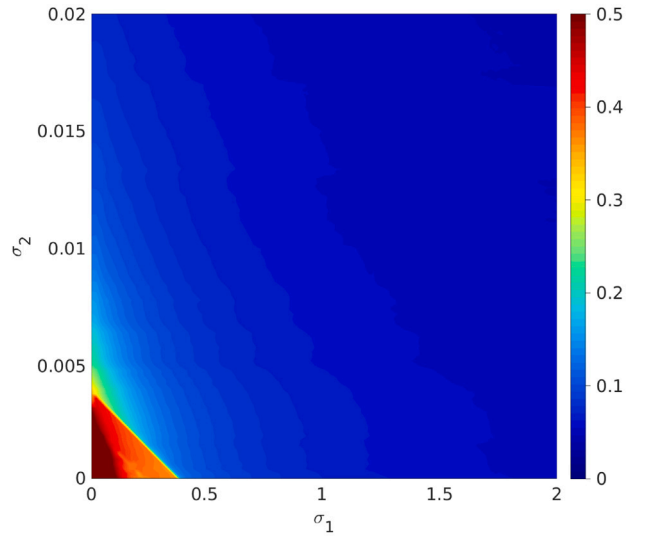

Fig. 7. Synchronization error map for $g^{(1)} = (\mathbf{x}_i, \mathbf{x}_j) = [0, y_j - y_i, 0]^T$ and $g^{(2)} = (\mathbf{x}_i, \mathbf{x}_j, \mathbf{x}_k) = [0, y_j^2 y_k - y_i^3, 0]^T$ as a function of the coupling strengths σ_1 and σ_2. This plot corresponds to the experiment (iv) referred in the main text. (For interpretation of the references to color in this figure legend, the reader is referred to the web version of this article.)

digital–analog electronic system composed of three Rössler oscillators whose coupling functions where adjusted in real time. With this experimental setup, we aimed to explore the higher-order relationships embedded within a simplicial complex of dimension $D = 2$. Our results show the complex behavior displayed by the whole system when multivariable and high-order coupling is introduced. We have seen that depending on the coupling configuration the synchronization region could be entered or reached, no matter if the coupling strengths are low or high. This kind of phenomena has been previously reported in (classical) complex networks with pairwise coupling, which allows to introduce a classification based on the way a network enters and reaches the synchronization manifold. Therefore it is possible to find analogies between the behavior of a complex networks with high order interactions (a simplicial complex in our case) and the behavior of class I (never reaching synchronization), II (synchronizing among a certain coupling strength) and III (synchronizing only at intermediate coupling strengths) systems as defined by the Master Stability Function. We believe that our results could be a starting point to further studies about dynamical simplicial complexes and, more generally, networks with nonlinear oscillators with higher-order interactions.

CRediT authorship contribution statement

V.P. Vera-Ávila: Validation, Methodology, Investigation, Data curation. **R.R. Rivera-Durón:** Writing – review & editing, Investigation, Data curation. **Miguel S. Soriano-Garcia:** Writing – review & editing, Investigation, Data curation. **R. Sevilla-Escoboza:** Writing – review & editing, Validation, Methodology, Investigation, Data curation, Conceptualization. **Javier M. Buldú:** Writing – original draft, Supervision, Project administration, Investigation, Conceptualization.

Declaration of competing interest

The authors declare that they have no known competing financial interests or personal relationships that could have appeared to influence the work reported in this paper.

Data availability

We have included a link with all datasets used in the paper.

Acknowledgments

The authors thank Prof. Stefano Boccaletti for fruitful discussions. J.M.B. acknowledges the support by Ministerio de Ciencia e Innovación, Spain under grant PID2020-113737GB-I00. R.S.E acknowledges support from the Consejo Nacional de Ciencia y Tecnología, Mexico call SEP-CONACYT/CB-2016–01, Grant No. 285909. V.P.V.A. acknowledges support from the Secretaria de Investigación y Posgrado (SIP) del Instituto Politécnico Nacional (IPN) Programa especial de consolidación de investigadores 2023, No. 20231415. R.R.R.D. acknowledges to Consejo Nacional de Humanidades, Ciencia y Tecnología, Programa de Estancias Posdoctorales por México, Grant I1200/331/2023.

Appendix. Supplementary material

For the numerical simulations of the simplicial complexes, a Runge–Kutta fourth-order method was employed with an integration step-size $h = 10^{-5}$ and 2^{16} steps. Figures Figs. 8–11 contain the synchronization errors of the numerical simulations for the different coupling scenarios.

The experimental time series recorded to calculate the synchronization error maps of Figs. 4–7 are available to download in [27–30].

The virtual instruments for each experiment are also available to download in [31]. In the RAR file, there are 2 main folders: Control-Acquisition and Coupling. Control-Acquisition folder contains the file named ControlGPD-2303S.vi necessary to control the programmable power supply (GW Instek GPD-2303S) via USB port; also, this file allows to acquire the time series using the data acquisition card (NI 6363). By the other hand, Coupling folder contains five files. The file SimplicialComplexes.lvproj corresponds to the complete project to configure and control the CompaqRIO (NI 9074). The four remaining files corresponds to the virtual instruments allow to calculate the possible scenarios of coupling functions $g^{(1)}$ and $g^{(2)}$ that we have mentioned in the main text. Namely, SimplextresnodosXX.vi, SimplextresnodosXY.vi, SimplextresnodosYX.vi, and SimplextresnodosYY.vi correspond to experiments (i), (ii), (iii), and (iv), respectively. Two important points must be considered: (a) these uploaded files work jointly, i.e., all files are necessary to reproduce the experiment; and (b) the same aforementioned hardware is necessary in order to reproduce the experiment.

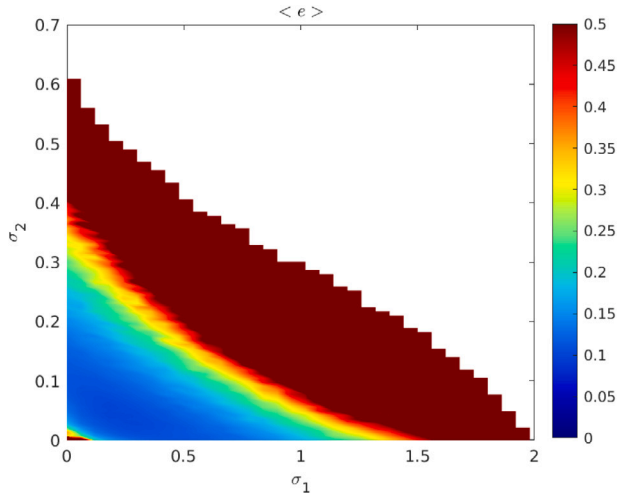

Fig. 8. Synchronization error map obtained by numerical simulations for $g^{(1)}(\mathbf{x}_i, \mathbf{x}_j) = [x_j - x_i, 0, 0]^T$ and $g^{(2)}(\mathbf{x}_i, \mathbf{x}_j, \mathbf{x}_k) = [x_j^2 x_k - x_i^3, 0, 0]^T$ as a function of the coupling strengths σ_1 and σ_2. This plot corresponds to the experiment (i) referred in the main text.

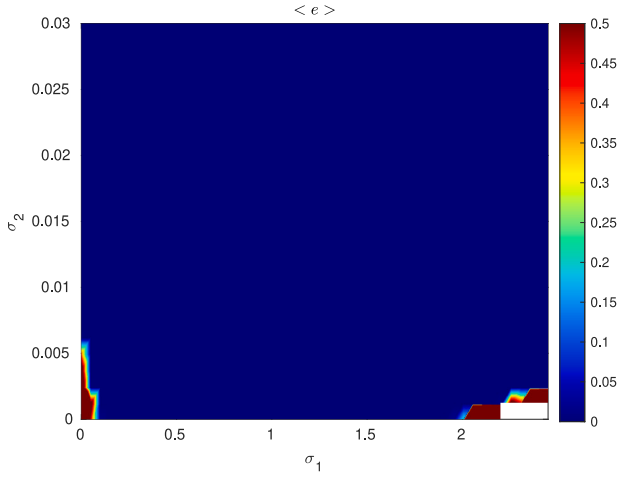

Fig. 9. Synchronization error map obtained by numerical simulations for $g^{(1)} = (\mathbf{x}_i, \mathbf{x}_j) = [x_j - x_i, 0, 0]^T$ and $g^{(2)} = (\mathbf{x}_i, \mathbf{x}_j, \mathbf{x}_k) = [0, y_j^2 y_k - y_i^3, 0]^T$ as a function of the coupling strengths σ_1 and σ_2. This plot corresponds to the experiment (ii) referred in the main text.

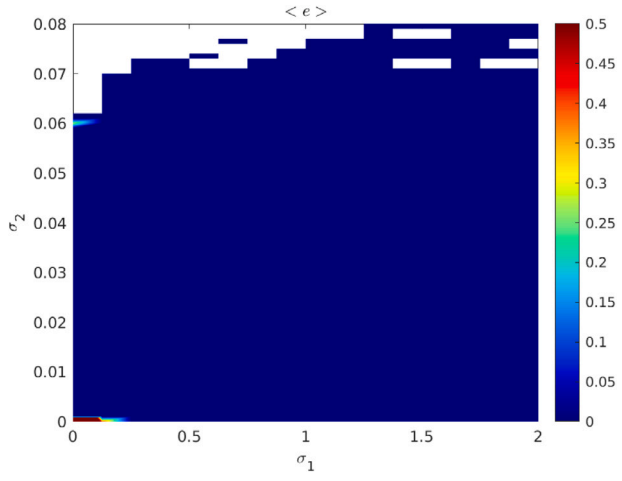

Fig. 10. Synchronization error map obtained by numerical simulations for $g^{(1)} = (\mathbf{x}_i, \mathbf{x}_j) = [0, y_j - y_i, 0]^T$ and $g^{(2)} = (\mathbf{x}_i, \mathbf{x}_j, \mathbf{x}_k) = [x_j^2 x_k - x_i^3, 0, 0]^T$ as a function of the coupling strengths σ_1 and σ_2. This plot corresponds to the experiment (iii) referred in the main text.

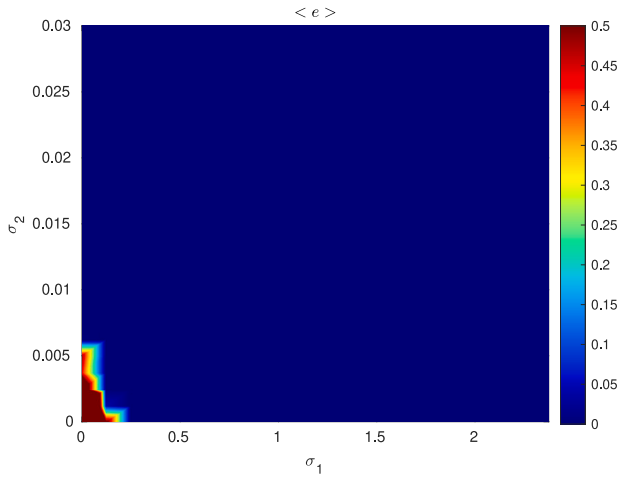

Fig. 11. Synchronization error map obtained by numerical simulations for $g^{(1)} = (\mathbf{x}_i, \mathbf{x}_j) = [0, y_j - y_i, 0]^T$ and $g^{(2)} = (\mathbf{x}_i, \mathbf{x}_j, \mathbf{x}_k) = [0, y_j^2 y_k - y_i^3, 0]^T$ as a function of the coupling strengths σ_1 and σ_2. This plot corresponds to the experiment (iv) referred in the main text.

References

[1] Pikovsky A, Rosenblum M, Kurths J. Synchronization: a universal concept in nonlinear science. Cambridge: Cambridge University Press; 2001.

[2] Newman M. Networks: an introduction. Oxford University Press; 2018.

[3] Bullmore E, Sporns O. Complex brain networks: graph theoretical analysis of structural and functional systems. 2009.

[4] Papo D, Buldú JM, Boccaletti S, Bullmore ET. Complex network theory and the brain. Philos Trans R Soc B 2014;3691653:20130520.

[5] Del Sol A, Fujihashi H, O'Meara P. Topology of small-world networks of protein–protein complex structures. Bioinformatics 2005;21(8):1311–5.

[6] Borge-Holthoefer J, Arenas A. Semantic networks: Structure and dynamics. Entropy 2010;12(5):1264–302.

[7] Barabási AL, Jeong H, Néda Z, Ravasz E, Schubert A, Vicsek T. Evolution of the social network of scientific collaborations. Phys A 2002;311(3–4):590–614.

[8] Bianconi G. Higher-order networks. Cambridge University Press; 2021.

[9] Boccaletti S, De Lellis P, del Genio CI, Alfaro-Bittner K, Criado R, Jalan S, Romance M. The structure and dynamics of networks with higher order interactions. Phys Rep 2023;1018:1–64.

[10] Battiston F, Amico E, Barrat A, Bianconi G, Arruda GFerrazde, Franceschiello B, Kéfi SIacopiniI, Latora V, Moreno Y, Murray MM, Peixoto TP, Vaccarino F, Petri G. The physics of higher-order interactions in complex systems. Nat Phys 2021;17(10):1093–8.

[11] Bianconi G, Rahmede C. Emergent hyperbolic network geometry. Sci Rep 2017;7(1). http://dx.doi.org/10.1038/srep41974.

[12] Carletti T, Fanelli D, Nicoletti S. Dynamical systems on hypergraphs. J Phys: Complex 2020;1:035006.

[13] Carletti T, Giambagli L, Bianconi G. Global topological synchronization on simplicial and cell complexes. Phys Rev Lett 2023;130:187401.

[14] Majhi S, Perc M, Ghosh D. Dynamics on higher-order networks: a review. J R Soc Interface 2022;19:20220043.

[15] Iacopini I, Petri G, Barrat A, Latora V. Simplicial models of social contagion. Nature Commun 2019;10(1). http://dx.doi.org/10.1038/s41467-019-10431-6.

[16] Reitz M, Bianconi G. The higher-order spectrum of simplicial complexes: a renormalization group approach. J Phys Math Theor 2020;53(29):295001. http://dx.doi.org/10.1088/1751-8121/ab9338.

[17] Courtney O, Bianconi G. Generalized network structures: the configuration model and the canonical ensemble of simplicial complexes. Phys Rev E 2016;93(6). http://dx.doi.org/10.1103/physreve.93.062311.

[18] Courtney O, Bianconi G. Weighted growing simplicial complexes. Phys Rev E 2017;95(6). http://dx.doi.org/10.1103/physreve.95.062301.

[19] Torres J, Bianconi G. Simplicial complexes: higher-order spectral dimension and dynamics. J Phys Complex 2020;1(1):015002. http://dx.doi.org/10.1088/2632-072x/ab82f5.

[20] Gambuzza L, Patti F, Gallo L, Lepri S, Romance M, Criado R, , Boccaletti S. Stability of synchronization in simplicial complexes. Nature Commun 2021;12(1). http://dx.doi.org/10.1038/s41467-021-21486-9.

[21] Millán A. Geometry, topology and simplicial synchronization. 2021, http://dx.doi.org/10.48550/arxiv.2105.00943.

[22] Pecora LM, Carroll TL. Master stability functions for synchronized coupled systems. Phys Rev Lett 1998;80(10):2109.

[23] Vera-Ávila VP, Sevilla-Escoboza JR, Durón RR, Buldú JM. Dynamical consistency in networks of nonlinear oscillators. Chaos Solitons Fractals 2021;148:111017.
[24] Vera-Ávila VP, Sevilla-Escoboza R, Lozano-Sánchez AA, Rivera-Durón RR, Buldú JM. Experimental datasets of networks of nonlinear oscillators: Structure and dynamics during the path to synchronization. Data Brief 2020;28:105012.
[25] Vera-Ávila VP, Sevilla-Escoboza JR, Leyva I. Complex networks exhibit intermittent synchronization. Chaos 2020;30(10).
[26] Boccaletti S, Latora V, Moreno Y, Chavez M, Hwang DU. Complex networks: Structure and dynamics. Phys Rep 2006;424(4–5):175–308.
[27] Sevilla-Escoboza JR, Vera Avila VP, Rivera Duron RR, Buldú MJ. Experimental validation of simplicial complexes in multivariable coupled oscillators. In: Coupling: lineal (class III) vs noLineal (class III). Zenodo; 2023.
[28] Sevilla-Escoboza JR, Vera Avila VP, River R, Buldú MJ. Experimental validation of simplicial complexes in multivariable coupled oscillators. In: Coupling: lineal (class III) vs noLineal (class II). Zenodo; 2023.
[29] Sevilla-Escoboza JR, Vera Avila VP, Rivera Duron RR, Buldú MJ. Experimental validation of simplicial complexes in multivariable coupled oscillators. In: Coupling: lineal (class II) vs noLineal (class III). Zenodo; 2023.
[30] Sevilla-Escoboza JR, Vera Avila VP, Rivera Duron RR, Buldú MJ. Experimental validation of simplicial complexes in multivariable coupled oscillators. In: Coupling: lineal (class II) vs noLineal (class II). Zenodo; 2023.
[31] Sevilla-Escoboza JR, Vera Avila VP, Rivera Duron RR, Buldú MJ. Experimental validation of simplicial complexes in multivariable coupled oscillators. Zenodo; 2024, http://dx.doi.org/10.5281/zenodo.10761796.